ARTICLE   OPEN

FK228 reshapes tumor microenvironment to enhance anti-PD-L1 efficacy

Liang Gong [1,2], Lu Tian [1,3], He Li[2,3], Kexuan Zhou[2,3], Haocheng He[1,2], Shuai Xiao[1], Yizhun Zhu [3], Zhicheng Gong [4✉], Kaisa Cui [4✉] and Youming Zhang [1,2,5✉]

The lack of a favorable tumor immune microenvironment (TIME) results in limited response rates to immune checkpoint blockade (ICB) across human solid tumors, necessitating the development of novel combination strategies. In this study, we repurposed FK228, an US FDA-approved histone deacetylase inhibitor that is used clinically in non-solid tumor treatment, as a novel ICB sensitizer in solid tumors and revealed the diverse regulatory functions of FK228 in the TIME. FK228 serves as a novel necroptosis inducer in cancer cells by triggering endoplasmic reticulum stress. This in turn enhances the immunogenicity of cancer cells and increases the infiltration of tumor-killing immunocytes, including $CD8^+$ T and natural killer cells, particularly activating tumor-infiltrated $CD8^+$ T cells. Meanwhile, FK228 treatment shifts macrophages toward the pro-inflammatory phenotype. Moreover, the combined use of FK228 and a PD-L1 inhibitor significantly delay tumor growth and extend the survival of tumor bearing mice. Overall, our findings reveal new possibilities for the clinical application of FK228 in solid tumors and underscore the critical role of histone deacetylases in maintaining the immune-unfavorable TIME.

INTRODUCTION

FK228, also known as romidepsin, is a small-molecule agent developed successfully by Celgene Co. Ltd. and was first approved by the US FDA in 2009 for the clinical treatment of cutaneous and peripheral T cell lymphoma [1, 2]. As a histone deacetylase (HDAC) inhibitor, FK228 can initiate the expressions of the epigenetically silenced genes to markedly hamper the proliferation of tumor cells in vitro and in vivo [3], which is achieved through the cell cycle and mitotic arrest by directly inhibiting the activities of HDAC1, HDAC2, HDAC4, and HDAC6 [4]. Currently, the single doses of FK228 used for clinical treatment are very high and relatively expensive, resulting in low clinical benefits for numerous patients. Therefore, our group previously focused on increasing the yield of FK228 to fulfill a desire [5]. On the basis of our original *Burkholderia*-specific recombineering system technology, we obtained FK228 with a 3-fold greater yield than the previously reported highest yield [5]. However, although FK228 has been successfully applied in the clinical treatment of non-solid tumors and we have improved its production, it has not yet received clinical approval for the treatment of solid tumors.

Previous clinical trials have shown that single-agent FK228 treatment has only moderate therapeutic effects on solid tumors, such as colorectal cancer [6], prostate cancer [7], and renal cancer [8]. Differ from non-solid tumors, such as lymphomas and hematomas, solid tumors have complex tumor microenvironments, and changes in their characteristics and status determine

the progression or regression of solid tumors [9]. In addition to cell cycle arrest induction in tumor cells, accumulating evidence has shown that HDAC inhibitors (HDACis) influence tumor immune microenvironment (TIME) regulation, such as enhancing the infiltration and activation of the $CD8^+$ T cells by the pan-HDACi vorinostat (SAHA) or LBH589 [10, 11], abolishing the immunosuppression microenvironment *via* the SAHA-reducing activity of regulatory T cells (Tregs) or entinostat reprogramming of tumor-infiltrating myeloid-derived suppressor cells (MDSCs) [12, 13]. PD-L1 plays an important role in tumor immunity and serves as the most prominent and effective target for immune checkpoint blockade (ICB) [14]. Previous studies have shown that FK228, a HDACi, promotes the expression of PD-L1 in solid tumor cells [15, 16], indicating that FK228 regulates the TIME. In addition, FK228 can increase T cell infiltration into lung cancer [17]. Nevertheless, few studies have revealed the TIME landscape of solid tumors after FK228 treatment. Moreover, there are no reports uncovering the mechanism how FK228 regulates the TIME.

Single-cell RNA sequencing (scRNA-seq) is one of the most effective approaches for understanding the TIME [18, 19]. We previously also used scRNA-seq technology to characterize the immune landscapes of the solid tumor [20]. In this study, we first explored the type of tumor cell death caused by FK228. The TIME landscapes in three solid tumor-transplanted models treated with FK228 were subsequently characterized using scRNA-seq to further analyze whether FK228-induced tumor cell death could

alter the TIME. Moreover, we investigated the mechanism of FK228-induced changes in the TIME, and analyzed the sensitivity of solid tumors to a PD-L1 inhibitor *via* FK228 treatment. Our study provides new insights into the use of FK228 in solid tumor treatments and reveals a novel mechanism by which FK228 remodels the TIME. This work provides guidance for the clinical treatment of solid tumors with FK228.

MATERIALS AND METHODS
Materials
The antibodies and other commercial reagents used are listed in Table S1.

Cell culture and animals
Mouse colorectal cancer MC38 and CT26 cells, mouse mononuclear macrophages RAW264.7 cells were purchased from the Mcellbank (Shanghai, China). Mouse breast cancer 4T1 cells, and human breast cancer MDA-MB-231, MDA-MB-436, MDA-MB-468 cells were obtained from the Pricella (Wuhan, China). All cell lines were confirmed by a short tandem repeat (STR) identification. MC38, RAW264.7, MDA-MB-231, and MDA-MB-436 cells were cultured in DMEM medium (Sigma, Cat# D6429) suppled with 10% FBS (Sigma, Cat# F8687 or MIKX, Cat# MK1123) and 1% penicillin-streptomycin (Beyotime, Cat# C0222). CT26 and 4T1 cells were incubated in RPMI1640 (Sigma, Cat# R8758) containing 10% FBS and 1% penicillin-streptomycin. MDA-MB-468 cells were grown in L15 (HyClone, Cat# SH30525.01) containing 10% FBS and 1% penicillin-streptomycin. All these cells were incubated at conditions of 37 °C in humidified 5% CO_2 atmosphere. Two types mice, including C57BL/6 and BALB/c mice (5 weeks, female) were purchased from Zhuhai Bestest Biotechnology Co., Ltd (Zhuhai, China).

Evaluation of FK228-induced cell death types
The 7-amino-actinomycin D (7-AAD) staining was used to detect the death of mouse solid tumor cells treated with FK228 (MCE, Cat# HY-15149). Briefly, MC38, CT26 or 4T1 cells (1×10^5 cells/well) were cultured in 6-well plates, followed by DMSO (Ctrl group) or FK228 (at IC_{50} concentration) treatment for 24 h, respectively. These cells, a mixture of both live and dead cells, were then collected, washed and incubated with 100 μL 1 × Assay Buffer containing 5 μL 7-AAD Staining Solution (Vazyme, Cat# A213) at room temperature for 10 min. The death cell rates (7-AAD-positive cells) were assessed by BD LSRFortessa Cell Analyzer (BD, USA). For cell death pathways, MC38, CT26 or 4T1 cells (3×10^3 cells/well) were seeded into 96-wells plates, respectively. After cell adherence overnight, these cells were treated with FK228 under IC_{50} concentration synergized with DMSO or different cell death inhibitors for 24 h. The cell viability was then determined by CCK-8 (ApexBio, Cat#K1018).

Colony-formation assay
Colony-formation assay was based on our previous works [21, 22]. Tumor cells (1000 cells/well) were cultured in 6-well plates for 14 days, then treated with FK228 under IC_{50} concentration. Prior to photograph, the colony was stained with crystal violet (Beyotime, Cat #C0121). DMSO treatment served as control (Ctrl).

Luminex platform analyses
Cell-free supernatants from FK228-treated tumor cells were collected and send to Shanghai UNIV Biotechnology Co., Ltd. (Shanghai, China). Multiple cytokines and/or chemokines were analyzed using Bio-Plex Pro Mouse Chemokine Panel 31-Plex (Bio-Rad, Cat# 12009159). Their concentrations were determined by Luminex X-200 (Luminex, USA). DMSO treatment served as control (Ctrl).

ATP release detection
Extracellular ATP from FK228-treated MC38, CT26, and 4T1 cells was quantified using Enhanced ATP Assay Kit (Beyotime, Cat# S0027) according to the manufacturer's instructions, respectively. After prepared the samples, the value was measured using a Synergy H11 microplate reader (Biotech, USA). DMSO treatment served as control (Ctrl).

Calreticulin (CRT) surface-location assay
MC38, CT26, and 4T1 cells were grown in 6-well plates at a density of 1 × 10^5 cells per well, and treated with FK228 under IC_{50} concentration for 12 h, respectively. These cells were obtained and washed with DPBS. Next, both anti-CRT antibody (HUABIO, Cat# ET1608-60) and DyLight 594-conjugated Goat-anti-Rabbit IgG (H + L) Secondary Antibody (Thermo, Cat# 35560) were used to label FK228-treated tumor cells without the damaged plasma membrane. The translocation of CRT was detected and observed by BD LSRFortessa Cell Analyzer or AX confocal laser scanning microscope (Nikon, Japan), respectively. DMSO treatment served as control (Ctrl).

Gold-standard in vivo vaccination assay
The vaccination assay was performed in line with previous studies [23, 24]. The tumor vaccines derived from FK228-killed MC38, CT26, and 4T1 cells were prepared. These dead cells were injected into the left flank of immunocompetent C57BL/6 or BALB/c mice, respectively. After 7 days, the homologous live tumor cells (1×10^5 cells/mouse) were inoculated into the right flank of above immunized mice. Both PBS and freeze-thawed tumor cells immunization group served as controls. Subsequently, tumor growth and incidence were recorded once every three days with calipers, and was calculated using the standard formula (length × width × width/2).

Animals therapy
C57BL/6 or BALB/c mice were subcutaneously injected with 4×10^5 MC38, CT26, or 4T1 cells in their right armpit of the forelimb to construct subcutaneous transplant tumors, respectively. These tumor-bearing mice were injected with FK228 (0.5 mg/kg) *via* the tail vein every 2 days (5 times in total), when the tumor volume attained to approximately 50 mm³. All FK228-monotherapeutic mice were humanely sacrificed and the tumor tissues were excised for further scRNA-seq analyses. DMSO with an equal volume of FK228 diluted in PBS acted as ctrl (control) group. For combination therapy, the immunologically cold CT26- or 4T1-harboring mouse models were established [25]. Then, these mice were divided randomly into four groups, including DMSO+IgG, DMSO + @PD-L1, FK228+IgG, FK228 + @PD-L1. According to the grouping protocols, the administrations were performed by intravenous injection with a dose of 0.5 mg/kg FK228 and/or 200 μg/mouse anti-PD-L1 (Bioxcell, Cat# BE0101) or IgG isotype control (Bioxcell, Cat# BE0090). After once treatment every 2 days (5 times in total), these tumors were dissected, weighed, and photographed, following by scRNA-seq. In addition, the tumor size was monitored and calculated using the same method as described above during the treatment period. Tumor diameter of 1.5 cm in any direction and its size of 1500 mm³ were considered as humane endpoint of tumor-bearing mice in therapeutic studies.

Flow cytometry
The infiltration of immune cells in subcutaneous tumors was determined according to our previous approaches [26, 27]. The harvested tumor tissues with therapy were disaggregated using enzyme digestion solution containing type I collagenase (1 mg/mL), hyaluronidase (200 μg/mL) and DNase I (150 μg/mL) at 37 °C for 1 h. After the single-cell suspensions were filtered through 70 μm cell strainer and performed red blood lysis using Red Blood Cell Lysis Buffer (MIKX, Cat# CE371), the lymphocyte was isolated using Tumor Tissue Mononuclear Cell Separation Solution (Solarbio, Cat# P4740). After labeled with Fixable Viability Stain 440UV (1:1000, BD, Cat# 566332) to exclude dead cells, these single lymphocytes were blocked with Rat Anti-Mouse CD16/CD32 (1 μg per 1×10^6 cells, BD, Cat# 553141) at 4 °C for 10 min, and stained with different flow cytometry antibodies for 30 min at 4 °C. For intracellular antigens (cytokine), before surface-stained cells were fixed and permeabilized using Intracellular Fixation & Permeabilization Buffer (Invitrogen, Cat# 88-8824-00), cells were stimulated with Leukocyte Activation Cocktail (BD, Cat# 550583) for 5 hours at 37 °C. Following this, the cells were subjected to blocking before undergoing antibody labeling. Finally, the stained cells were detected by BD LSRFortessa Cell Analyzer.

Multiplex immunofluorescence
Three type immune cells in tumor tissues, including CD8+ T cells, pro-inflammatory (M1-like) or anti-inflammatory (M2-like) Mφ, were visualized using multiplex immunofluorescence based on our technology [20]. The tumor tissues were sectioned, fixed, penetrated, and primary antibody labeling. Subsequently, Alexa Fluor 488 conjugated Goat-anti-Rabbit IgG (Servicebio, Cat# GB25303) was used to label CD8+ T cells, and HRP-conjugated Goat-anti-Rabbit IgG (Servicebio, Cat# GB23303) and TSA Kit (Servicebio, Cat# G1236) was used to label Mφ. The slides were observed by Zeiss LSM980 or AX confocal laser scanning microscope. Ctrl (control)

group represents the tumors from mice receiving the treatment with DMSO with an equal volume of FK228 diluted in PBS.

Co-culture experiments

To investigate the in vitro effects of FK228 on tumor-associated macrophages (TAMs), a transwell co-culture system of RAW264.7 cells (3×10^5 cells) and tumor cells (1×10^5 cells) was employed, wherein RAW264.7 or tumor cells were cultured in the lower or upper chamber, respectively. Following overnight attachment, FK228 was added to the upper chamber, and the cells were cultured for 48 h. Subsequently, these cells from the lower chamber were collected, labeled with the IL-1β, and analyzed using BD LSRFortessa Cell Analyzer. DMSO treatment served as control (Ctrl).

In order to assess whether FK228 directly influences pro-inflammatory macrophage polarization. Using the abovementioned co-culture setup, RAW264.7 cells were first induced into M2-like macrophages for 48 h. The upper chamber was then removed, and FK228 was added directly to the induced M2-like TAMs in the lower chamber. Finally, these cells were detected using flow cytometry. DMSO treatment served as control (Ctrl).

Western blotting

The expressions of the related proteins were analyzed according to our methods [28, 29]. In brief, A mixture of both live and dead cells treated with FK228 or DMSO (Ctrl group) was lysed using RIPA lysis buffer (Beyotime, Cat# P0013C) suppled with Protease Inhibitor Cocktail (MCE, Cat# HY-K0010) and PMSF (Beyotime, Cat# ST506). After determining protein concentration, equal amounts of protein extracts were subjected to SDS-PAGE gel electrophoresis (Sangon, Cat# C661101) and then transferred to PVDF membrane (Vazyme, Cat# E801). Prior to corresponding primary antibodies incubation, the membranes were blocked with NcmBlot blocking buffer (New Cell & Molecular Biotech, Cat# P30500). Subsequently, the membranes with 3-times washes were incubated in HRP-conjugated secondary antibodies, followed by the band visualizations using ECL Chemiluminescence Kit (Vazyme, Cat# E422) under chemiluminescent system (Analytikjena, Germany).

ScRNA-seq assay

Tissues from tumor murine models were performed dissociation by experimental personnel in the laboratory of SeekGene Biotechnology Co., Ltd. (Beijing, China). Single-cell suspensions from samples were sorted by using CD45 MicroBeads (Miltenyi, Cat# 130-052-301) and then integrated cells following $CD45^+:CD45^- = 3:1$. The scRNA-seq libraries were prepared using the SeekOne® Digital Droplet (DD) Single Cell 3′ library preparation kit (SeekGene, Cat# K00202) and related platform following the manufacturer protocol and libraries sequencing was performed in an Illumina NovaSeq 6000. SeekSoul® Tools were used to proceed raw data and generated Unique Molecular Identifier (UMI) count matrices. The R package Seurat 4 was used to further processed and annotated scRNA-seq UMI count matrices data [30]. Ro/e approach was used to calculate the ratio of observed to expected cell numbers for each cell type in different treatment groups to quantify the preference of each cell type[31]. One cell type was identified as being enriched in a specific treatment group if Ro/e > 1, while < 1 indicates depletion. The expected cell numbers for each combination of cell types and treatment groups were obtained from the chi-square test. Transcription factor analysis of $CD8^+$ T cells was used the python package pySCENIC [32]. ER stress pathway gene sets were obtained from molecular signatures database (MSigDB, https://www.gsea-msigdb.org/gsea/msigdb/collections.jsp) and enrichment analysis was used the R package UCell [33].

Public data and statistical analysis

The transcriptomic data about human cancer cell lines treated with FK228 were downloaded (https://www.ncbi.nlm.nih.gov/geo/query/acc.cgi?acc=GSE133120) [34]. Statistical analyses were performed using GraphPad Prism 10 and R 4.3.0. Significant difference was executed and set as follow: *p-value < 0.05, **p-value < 0.01, ***p-value < 0.001, ****p-value < 0.0001, ns, no significant. The data were presented as the mean ± SD.

RESULTS

FK228 induces solid tumor cell necroptosis

FK228 can kill human solid tumor cells as previously described [5, 35]. Hence, we first explored whether FK228 can cause the

death of mouse solid tumor cells, including mouse colorectal cancer MC38 and CT26 cells, and mouse breast cancer 4T1 cells. As expected, we obtained lower IC_{50} values for the above three tumor cell lines (43.37 nM for MC38, 58.61 nM for CT26, and 13.49 nM for 4T1) (Fig. S1A), and observed extensive cell death in the FK228-supplemented group compared with Ctrl group (DMSO treatment) (Fig. 1A). These results were confirmed using 7-amino-actinomycin D (7-AAD) staining (Fig. 1B, C) and colony formation assays (Fig. S1B). Treatment with FK228 can increase both histone 3 and 4 acetylation levels in human cancer cells [36]. We also conducted histone acetylation assays in mouse solid cancer cells. In comparison with the Ctrl (DMSO treatments), the FK228 treatments significantly induced acetylation at different lysine sites, such as histone 3 at lysine 9 and 27 sites and histone 4 at lysine 8 and 16 sites (Fig. S1C).

Next, we investigated the type of cell death induced by FK228. Multiple inhibitors for common cell death pathways, including Z-VAD-FMK for apoptosis inhibition, necrostatin-1 for necroptosis inhibition, ferrostatin-1 for ferroptosis inhibition, disulfiram for pyroptosis inhibition, and 3-methyladenine for autophagy inhibition, were used to prevent the cell death [37]. Obviously, necrostatin-1 significantly reversed the reductions in the viability of MC38, CT26 and 4T1 cells during FK228 treatment compared with other inhibitors (Fig. 1D), suggesting that FK228 can trigger solid tumor cell necroptosis. To verify this hypothesis, we analyzed necroptosis markers in these FK228-treated cell lines using western blotting. The phosphorylation of the pseudokinase mixed lineage kinase-like domain (MLKL), an inducer of necroptosis [38], was obviously increased in the above three solid tumor cell lines after exposure to FK228 at both 10- and 12-hours (Figs. 1E and S2). Additionally, we observed the enhanced RIPK1 and RIP3 phosphorylation, which are upstream molecules that induce the phosphorylation of MLKL (Figs. 1E and S2). When necroptosis occurs, the cells release massive amounts of cytokines and/or chemokines [39]. Subsequently, we determined the concentrations of chemokines involved in FK228-induced necroptosis in these three solid tumor cell lines via the Luminex platform. These findings showed that FK228 can stimulate the release of many inflammatory chemokines, such as CX3CL1, CXCL10 and so on (Fig. S1D).

Necroptotic solid tumor cells treated with FK228 trigger immunogenic cell death

Encouraged by the release of inflammatory factors from the FK228-induced tumor cell necroptosis, we speculated that FK228 administration stimulates immunogenic cell death (ICD) in solid tumor cells. To corroborate these results, we evaluated the ICD hallmarks in FK228-treated MC38, CT26 and 4T1 cells in vitro. The features of ICD commonly include upregulation, cell-surface expression, or release of immunostimulatory damage-associated molecular patterns (DAMPs) by the dying tumor cells [40]. ATP, a chemoattractant signal released into the extracellular environment, can recruit and activate antigen-presenting cells (APCs) [23]. As conjectured, we detected a significant increase in ATP release from tumor cells treated with FK228 relative to Ctrl (DMSO treatment) (Fig. 2A). In addition, another ICD marker, calreticulin (CRT), is overexpressed and translocated onto the membrane of the dying tumor cells, which serves as an "eat me" signal to facilitate identification and phagocytosis by APCs [23]. A robust increase in CRT expression was observed in FK228-treated MC38, CT26 and 4T1 cells compared with Ctrl (DMSO treatment) using western blotting (Figs. 2B and S3). Further immunofluorescence and flow cytometry analyses confirmed the cell-surface CRT expressions after FK228 exposure (Fig. 2C, D). According to previous reports, drug-killed tumor cells as an antitumor vaccine is the gold standard for determining whether drugs can induce ICD in cancer cells [23, 24, 41]. We next investigated the immunogenicity of dead tumor cells induced by FK228. After three tumor
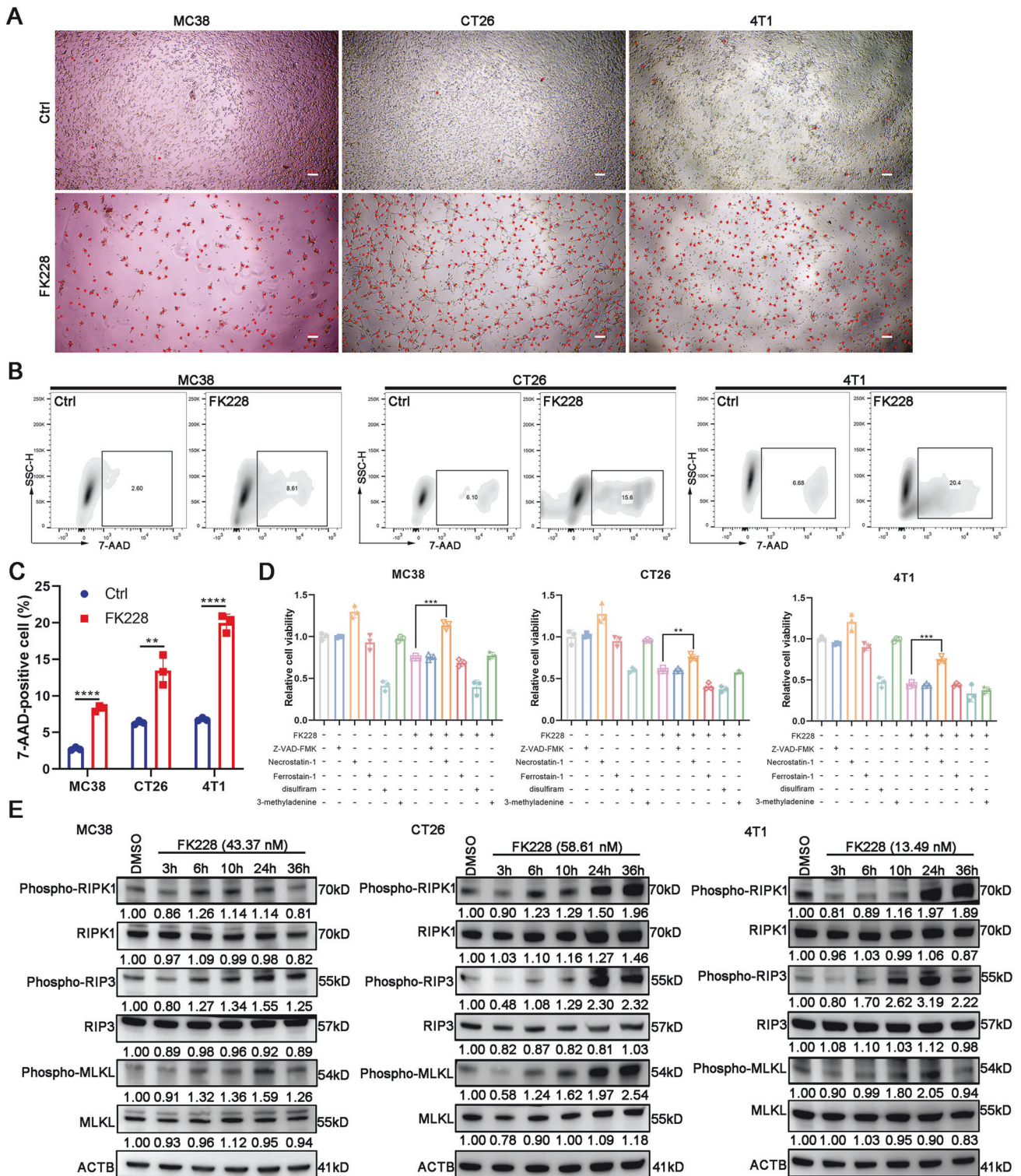
Fig. 1 FK228 facilitates the direct death of solid tumor cells by inducing necroptosis. A Representative images of cell death in MC38, CT26, and 4T1 with 43.37 nM, 58.61 nM, 13.49 nM FK228 treatment for 48 h, respectively. Ctrl indicates DMSO treatment. Scale bar, 100 μm. **B**, **C** Quantification of cell death using 7-amino-actinomycin D (7-AAD) staining in three mouse solid tumor cells treated with FK228 under its indicated IC_{50} for 24 h. Ctrl indicates DMSO treatment. Significant difference was executed using Student's t-test. **D** Determination of cell death pathways mediated by FK228 based on the rescue with different cell death inhibitors. Three mouse solid tumor cells were treated with or without FK228 under its indicated IC_{50} for 24 h in combination with the apoptosis inhibition Z-VAD-FMK (40 μM), the necroptosis inhibition necrostatin-1 (80 μM), the ferroptosis inhibition ferrostatin-1 (2 μM), the pyroptosis inhibition disulfiram (5 μM), and the autophagy inhibition 3-methyladenine (10 μM), and then analyzed using CCK-8. Significant difference was executed using Student's t-test. **E** The analysis for markers of necroptosis in three solid tumor cell lines treated with FK228 for different times using western blotting.
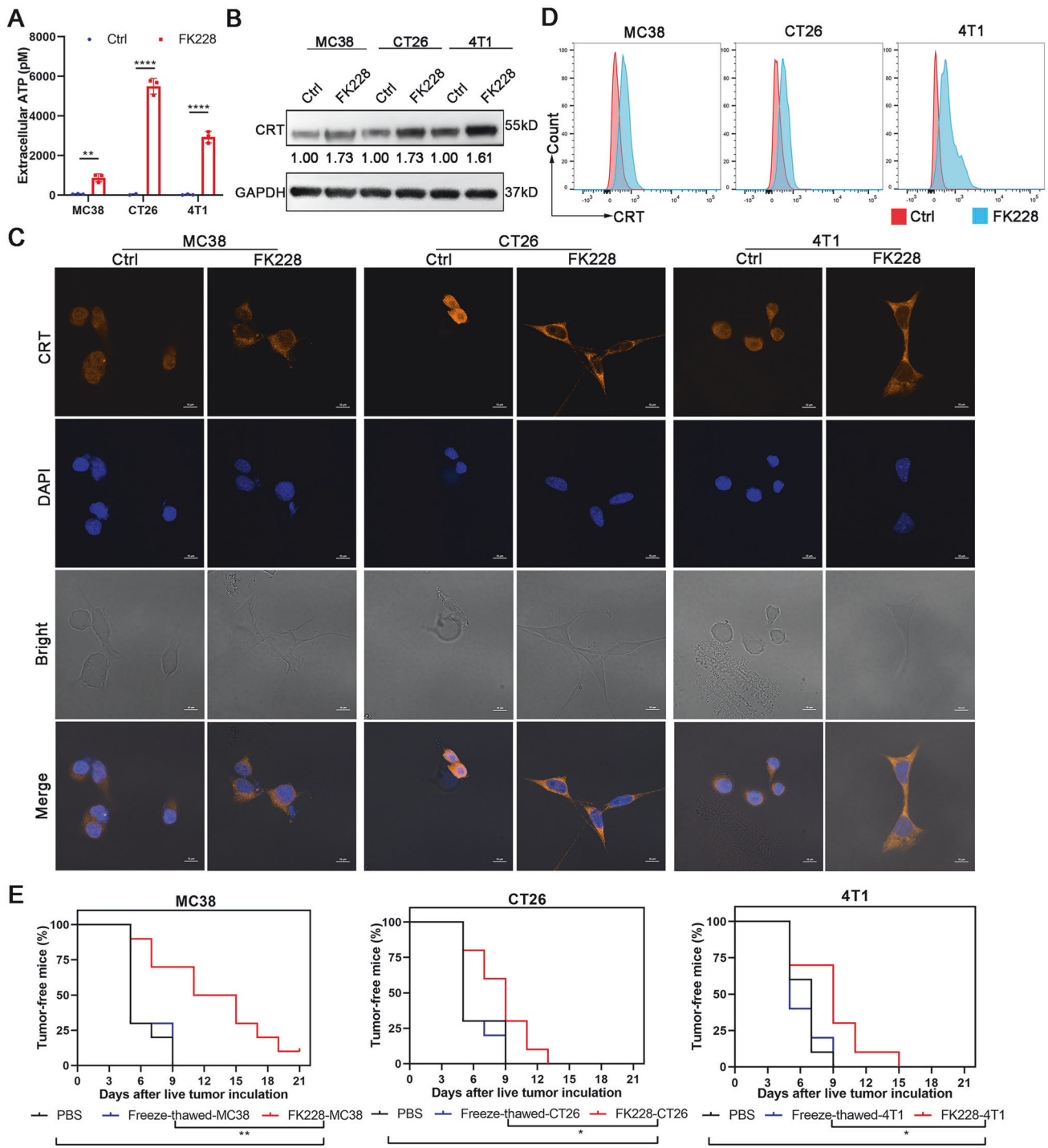
Fig. 2 **FK228-mediated necroptosis of solid tumor cells evokes immunogenic cell death (ICD). A** Extracellular ATP content released by FK228-treated three solid tumor cells under its indicated IC_{50} for 24 h. Ctrl indicates DMSO treatment. Significant difference was executed using Student's *t*-test. **B** Western blotting showing cellular calreticulin (CRT) expressions in three solid tumor cells with FK228-treatment using its indicated IC_{50} for 24 h. Ctrl indicates DMSO treatment. **C, D** CRT surface-localization using confocal fluorescence images (**C**) and flow cytometry analyses (**D**) in FK228-treated three solid tumor cells with its indicated IC_{50} for 24 h. Ctrl indicates DMSO treatment. Scale bar, 10 μm. **E** Gold-standard in vivo vaccination assay for ICD investigation. Three solid tumor cells were pretreated with indicated IC_{50} FK228, or freeze-thawed, followed by subcutaneous inoculation into corresponding mice as a vaccine ($n = 10$). After 7 days later, these mice were rechallenged with live corresponding tumor cells. Shown are the percentages of tumor-free mice 21 days after rechallenge. Significant difference was executed using Log-rank (Mantel–Cox) test.

cell lines were treated with FK228 in vitro, these dead cells were injected into the left flank of immunocompetent C57BL/6 or BALB/c mice. These mice were rechallenged with homologous live tumor cells that were inoculated into the right flank 7 days later.

Compared with those immunized with freeze-thawed tumor cells, the mice immunized with FK228-treated dead tumor cells exhibited significantly increased tumor-free survival (Fig. 2E). These results demonstrated FK228 as a bona fide ICD inducer.

FK228 promotes CD8$^+$ T cells infiltration and activation in solid tumors

Tumor ICD can globally reprogram the TIME [42]. Next, we constructed three syngenetic tumor mouse models, including MC38-engrafted C57BL/6 mice and CT26- or 4T1-bearing BALB/c mice, and conducted scRNA-seq to assess the TIME landscape of FK228 pre- and post-treated solid tumors (Fig. 3A). We performed quality control and annotated major cell types according to marker genes (Fig. S4A, B). Interestingly, we analyzed ICD-related indicators in cancer cells in vivo at the single-cell transcriptome level. In line with the abovementioned findings, the expressions of most DAMPs were significantly upregulated after FK228 treatment versus solvent control (DMSO treatment) (Fig. S4C).

T cell subpopulations and their infiltration play critical roles in antitumor therapy. We identified T cells from the abovementioned scRNA-seq landscape, and further clustered and annotated them (Fig. S5A–D). CD8$^+$ T cells represent one of the most effective immune cell types for anticancer treatment in the TIME [26, 27, 43]. Our analyses presented that FK228 treatment obviously increased the number of tumor-infiltrating CD8$^+$ T cells in the three mouse models (Fig. 3B). Flow cytometry analysis of single cells isolated from tumor tissues treated with FK228 further confirmed the enhancing CD8$^+$ T cells (Figs. 3C and S6A). Tumor tissue slices also showed a significant increase in the infiltration of CD8$^+$ T cells in the FK228-treated group compared with the Ctrl (DMSO treatment) group (Figs. 3D and S7A). Besides the increased infiltration of CD8$^+$ T cells, its activation is required to achieve prominent antitumor therapy efficiency [44]. We next evaluated the cytotoxic granules expression of CD8$^+$ T cells in three FK228-treated mouse solid tumor models based on scRNA-seq analyses. Several genes expressing antitumor effector molecules, such as granzyme families and perforin, showed significant upregulation in the CD8$^+$ T cells of three FK228-treated mouse solid tumor models compared to the Ctrl (DMSO treatment) group (Fig. 3E). We then used flow cytometry and determined the higher CD8$^+$ T cell subpopulations expressing granzyme B (GZMB) and IFN-γ in three FK228-treated mouse solid tumor models than those in Ctrl (DMSO treatment) group (Fig. 3F and S6A). Moreover, to elucidate the putative upstream regulators of the CD8$^+$ T cell activations after FK228 treatment, we used pySCENIC to identify transcription factor regulons [32]. A series of transcription factor regulons were upregulated in CD8$^+$ T cells under FK228 administration (Figs. 3G and S5E), providing a potential explanation for stimulating cytotoxic granules expression in CD8$^+$ T cells after FK228 treatment.

FK228 induces pro-inflammatory phenotype of macrophage in solid tumors

Besides malignant cells, tumor-associated macrophages (TAMs) are the most abundant cell population in the TIME [45]. TAMs with pro-inflammatory (M1-like) or anti-inflammatory (M2-like) phenotype are considered to describe the functional diversity of macrophages (Mφs) [46]. We also isolated Mφs and other myeloid cells from the scRNA-seq results to further annotate each subtype (Fig. S8A–D). Notably, FK228 promoted pro-inflammatory Mφs and suppressed anti-inflammatory Mφs in three solid tumor models compared to Ctrl (DMSO treatment) group (Fig. 4A). In vitro co-culture of tumor cells and RAW264.7 cells showed a greater proportion of the pro-inflammatory Mφ phenotype in the FK228-treated group than in Ctrl (DMSO treatment) group (Fig. 4B). Subsequently, we observed the similar results in three solid tumor models treated with FK228 in vivo through flow cytometry (Figs. 4C and S6B) and multiplex immunofluorescence (Figs. 4D and S7B, C). To determine whether the Mφ phenotype in the TIME is directly affected by FK228, we directly utilized FK228 to treat TAMs derived from abovementioned co-culture system. FK228 significantly promoted TAM reprogramming into pro-inflammatory Mφs compared with that in the Ctrl (DMSO

treatment) group (Fig. 4E). Additionally, we detected the increasing neutrophils (Fig. S8E) and the reducing MDSCs (Fig. S8F) after FK228 administration. These findings revealed that FK228 can reprogram myeloid cells, especially Mφs.

FK228 improves the sensitivity of solid tumors to a PD-L1 blockade

Previous studies have illustrated that FK228 can promote the PD-L1 expression in carcinoma cells [15, 16]. We also confirmed the expression of PD-L1 in a series of human or mouse cancer cell lines after FK228 treatment (Fig. S9A). In addition, our scRNA-seq data displayed that the PD-L1 expression was obviously increased in cancer cells and Mφs after FK228 treatment (Fig. S9B-C). Intriguingly, the PD-1, a corresponding receptor of PD-L1, was obviously upregulated in total T cells and CD8$^+$ T cells after FK228 treatment (Fig. S9D, E). The flow cytometry assays corroborated the above sequencing results (Fig. S9F–H). Moreover, based on GSE133120 dataset [34], we also found the higher PD-L1 expression levels in FK228-incubated human cancer cell lines (Fig. S9I).

Although FK228-therapeutic solid tumors exhibit abundant anticancer immune cell infiltration and reprogramming, the enhancing PD-1/PD-L1 expression can drive the exhaustion of T cells [47]. Our previous work has shown that TAMs expressing PD-L1 are detrimental to the prognosis of patients with tumors [26]. To further improve the therapeutic effects of FK228 on solid tumors and evaluate the responsiveness of immune-cold tumors to ICB treatment by FK228 sensitization, we performed the combined treatment with anti-PD-L1 and FK228 in immunologically cold CT26-harboring mouse models (Fig. 5A). Compared with the control (DMSO + IgG) or monotherapy group, the combined FK228 and anti-PD-L1 therapy resulted in the most severe delayed tumor growth (Fig. 5B–D), indicating that FK228 could significantly enhance tumor sensitivity to PD-L1 inhibitors. Additionally, the median survival of these administrated mice within 30 days was 6, 10.5, 8, and 28 days in DMSO + IgG, DMSO + @PD-L1, FK228 + IgG, and FK228 + @PD-L1 group, respectively (Fig. 5E), suggesting that the combined therapy dramatically prolonged the survival periods of the mice. Surprisingly, four mice (total eleven mice) in the combination therapy group had their tumors completely regressed. Of note, no obvious weight loss was observed in any of the groups through monitoring the murine body weights during the course of the different agent administrations (Fig. S10A). In another immunologically cold 4T1-harboring mouse model, we also observed similar results in the combination therapy group (Fig. S11). Subsequently, we explored the TIME landscape of combination therapy for CT26 tumors via scRNA-seq (Fig. S10B–D), and further annotated each subpopulation of T cells and Mφ cells (Fig. S10E–H). The combination group presented the greatest infiltration of anticancer immune cells, such as pro-inflammatory Mφ, dendritic cell (DC), neutrophil, and CD8$^+$ T cells, as well the modest accumulation of anticancer natural killer (NK) cells (Fig. 5F). A remarkable decrease in anti-inflammatory Mφs was detected in tumors treated with FK228 combined with a PD-L1 inhibitor (Fig. 5F). We further confirmed several differences in immune cells, including pro-inflammatory Mφs, DC, NK, and CD8$^+$ T cells, in solid tumor after different therapeutic strategies via flow cytometry (Figs. 5G and S6). Multiplex immunofluorescence observations presented the changes in CD8$^+$ T cells and pro- and anti-inflammatory Mφs across the four treatment groups, which were similar to the results of the above scRNA-seq and flow cytometry methods (Figs. 5H, I and S7D, E). Interestingly, combination therapy can induce the strongest activation of CD8$^+$ T cell, boosting the potential secretion of cytotoxic granules, including those of the granzyme family and perforin (Fig. 5J). We determined the highest frequency of GZMB-positive CD8$^+$ T cells in combined therapeutic tumors (Figs. 5K and S6A). These results suggested that FK228 increases the sensitivity of solid tumors to PD-L1 therapy and has great potential for the treatment of solid tumors.
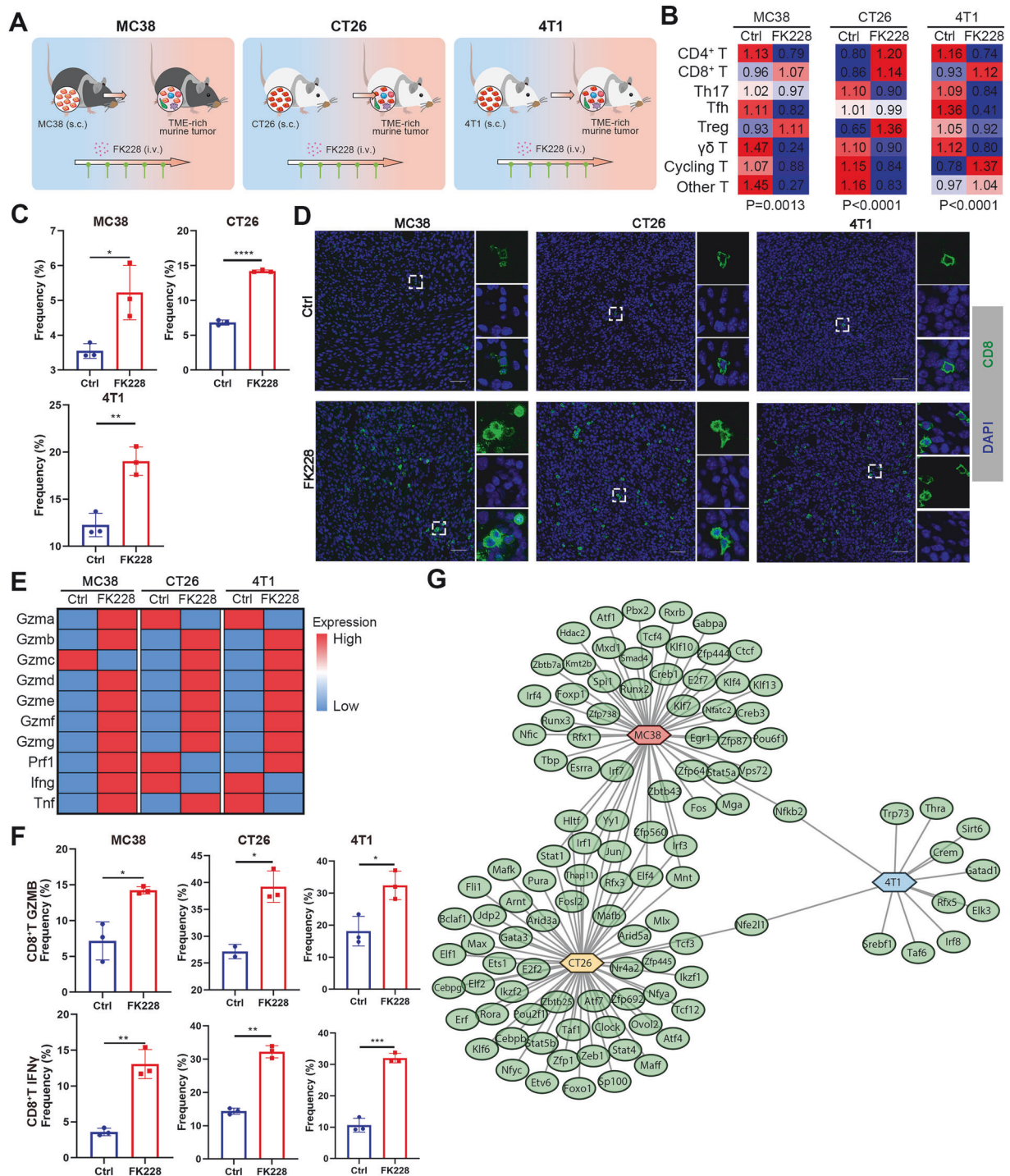
Fig. 3 FK228 treatments increase infiltration and activation of CD8$^+$ T cells in solid tumors. A A schematic depiction of the FK228 therapy in three subcutaneous tumor models. After tumor-bearing mice preparation with 4×10^5 tumor cells subcutaneous injection, they were intravenously injected with 0.1 mL FK228 (0.5 mg/kg) or DMSO with an equal volume of FK228 diluted in PBS ($n = 5$). **B** Ro/e heatmaps showing the FK228 treatment preference of each T cell subtype. Ctrl represents the tumors from the mice receiving DMSO treatment with an equal volume of FK228 diluted in PBS. Significant difference was executed using chi-square test. **C** Flow cytometry showing the relative amount of CD8$^+$ T cells in tumor tissues with or without FK228 treatments. Ctrl represents the tumors from the mice receiving DMSO treatment with an equal volume of FK228 diluted in PBS. Significant difference was executed using Student's t-test. **D** Representative immunofluorescence observation of CD8$^+$ T cells in tumor tissue slides from FK228 pre- or post-treated mice models. Ctrl represents the tumors from the mice receiving DMSO treatment with an equal volume of FK228 diluted in PBS. Scale bar, 50 μm. **E** Standardized mean expressions of cytotoxic granules in CD8$^+$ T cells grouped by FK228 pre- and post-treatment. Ctrl represents the tumors from the mice receiving DMSO treatment with an equal volume of FK228 diluted in PBS. **F** The relative amount of activated CD8$^+$ T cells with high expression of GZMB and IFN-γ in tumor tissues from FK228-treated mice. Ctrl represents the tumors from the mice receiving DMSO treatment with an equal volume of FK228 diluted in PBS. Significant difference was executed using Student's t-test. **G** Network of transcription factor regulons that upregulated in FK228 treatment CD8$^+$ T cells.
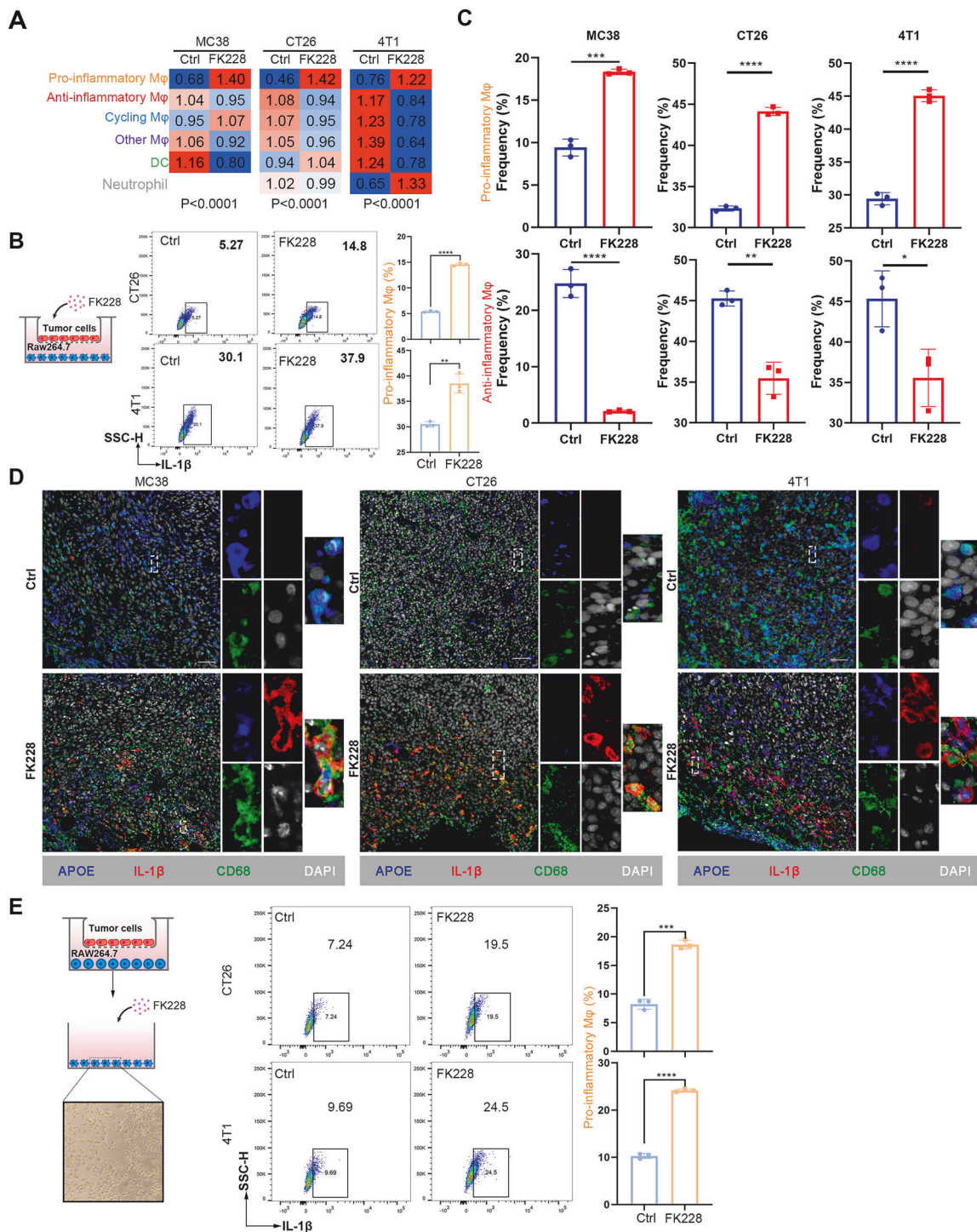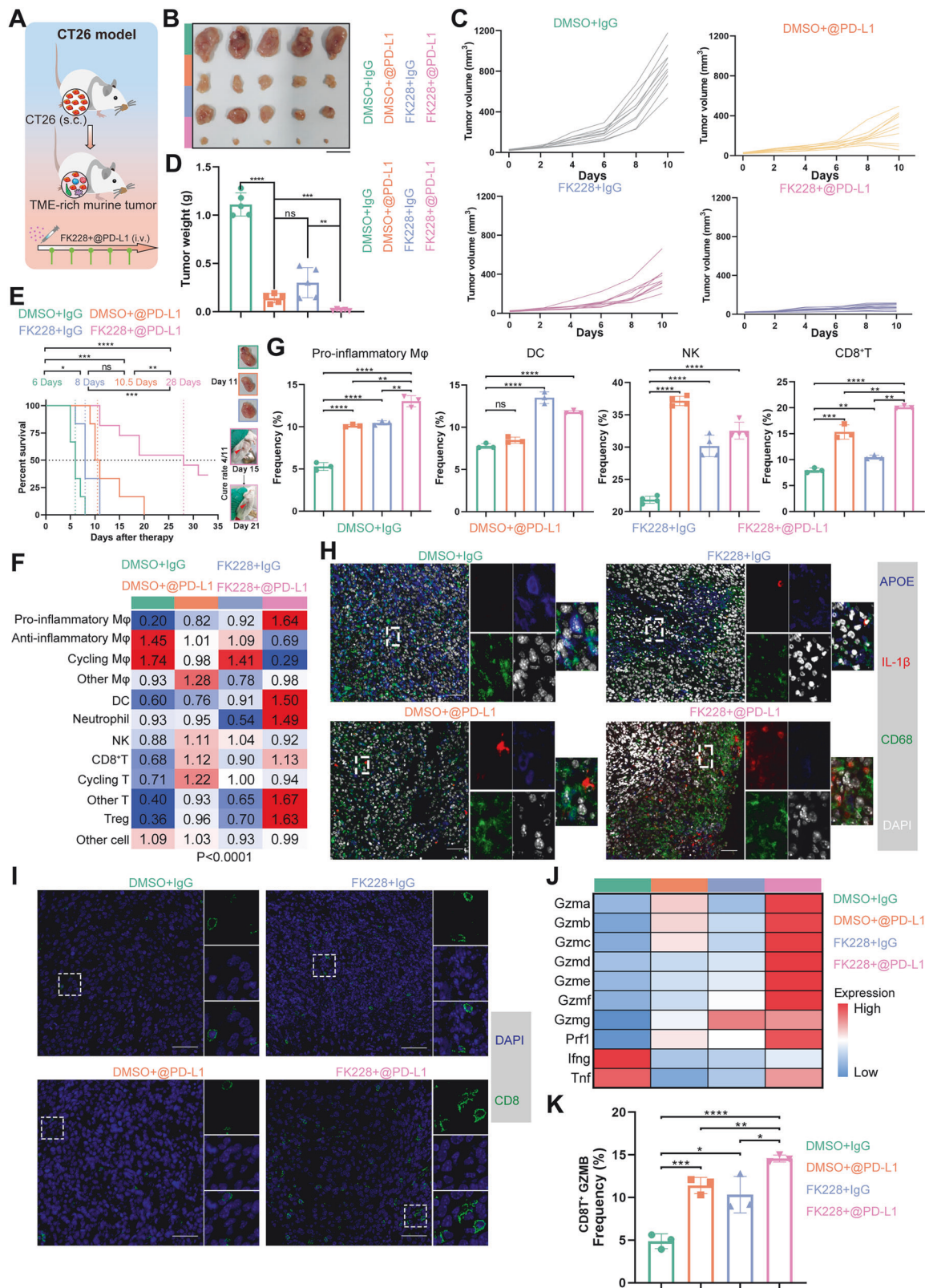
Fig. 4 FK228 reprograms tumor-associated macrophages (TAMs) in solid tumors. A Ro/e heatmaps showing the FK228 treatment preference of each macrophage subtype. Ctrl represents the tumors from the mice receiving DMSO treatment with an equal volume of FK228 diluted in PBS. Significant difference was executed using chi-square test. **B** Effects of FK228 on TAMs polarization in vitro co-culture between tumor cells and RAW264.7 cells. A transwell co-culture system of RAW264.7 cells (3×10^5 cells, cultured in the lower chamber) and tumor cells (1×10^5 cells, cultured in the upper chamber) was employed. After the FK228 supplement in the upper chamber for 48 h, the cells in the lower chamber were analyzed using flow cytometry. Ctrl indicates DMSO treatment. Significant difference was executed using Student's t-test. **C** The relative number of pro-inflammatory (M1-like) or anti-inflammatory (M2-like) Mφs in tumor tissues from mice with or without FK228 treatments based on flow cytometry. Ctrl represents the tumors from the mice receiving DMSO treatment with an equal volume of FK228 diluted in PBS. Significant difference was executed using Student's t-test. **D** Visualization of Mφs for pro-inflammatory (M1-like) or anti-inflammatory (M2-like) phenotype in tumor tissues in line with multiplex immunofluorescence image. Ctrl represents the tumors from the mice receiving DMSO treatment with an equal volume of FK228 diluted in PBS. Scale bar, 50 μm. **E** The direct reprogramming of FK228 to TAMs. After RAW264.7 cells were induced into M2-like Mφs, FK228 was added directly to the induced M2-like TAMs. These cells were detected using flow cytometry for pro-inflammatory Mφ. Ctrl indicates DMSO treatment. Significant difference was executed using Student's t-test.

Figure A: CT26 model. CT26 (s.c.) → TME-rich murine tumor. FK228+@PD-L1 (i.v.)

Figure B: tumor images for DMSO+IgG, DMSO+@PD-L1, FK228+IgG, FK228+@PD-L1

Figure C: Tumor volume (mm³) over Days for DMSO+IgG, DMSO+@PD-L1, FK228+IgG, FK228+@PD-L1

Figure D: Tumor weight (g)

Figure E: Percent survival (%) vs Days after therapy; 6 Days, 8 Days, 10.5 Days, 28 Days; Day 11, Day 15, Day 21; Cure rate 4/11

Figure F: Heatmap of cell frequencies across DMSO+IgG, DMSO+@PD-L1, FK228+IgG, FK228+@PD-L1

	DMSO+IgG	DMSO+@PD-L1	FK228+IgG	FK228+@PD-L1
Pro-inflammatory Mφ	0.20	0.82	0.92	1.64
Anti-inflammatory Mφ	1.45	1.01	1.09	0.69
Cycling Mφ	1.74	0.98	1.41	0.29
Other Mφ	0.93	1.28	0.78	0.98
DC	0.60	0.76	0.91	1.50
Neutrophil	0.93	0.95	0.54	1.49
NK	0.88	1.11	1.04	0.92
CD8+T	0.68	1.12	0.90	1.13
Cycling T	0.71	1.22	1.00	0.94
Other T	0.40	0.93	0.65	1.67
Treg	0.36	0.96	0.70	1.63
Other cell	1.09	1.03	0.93	0.99

P<0.0001

Figure G: Frequency (%) for Pro-inflammatory Mφ, DC, NK, CD8+T

Figure H: APOE, IL-1β, CD68, DAPI staining for DMSO+IgG, FK228+IgG, DMSO+@PD-L1, FK228+@PD-L1

Figure I: DAPI, CD8 staining for DMSO+IgG, FK228+IgG, DMSO+@PD-L1, FK228+@PD-L1

Figure J: Expression heatmap (High/Low) of Gzma, Gzmb, Gzmc, Gzmd, Gzme, Gzmf, Gzmg, Prf1, Ifng, Tnf

Figure K: CD8T+ GZMB Frequency (%)

FK228 promotes endoplasmic reticulum stress in solid tumor cells

Chemotherapy-induced ICD is often contributed by endoplasmic reticulum (ER) stress [48, 49]. To survey how FK228 induces necroptosis in solid tumor cells, thereby initiating global tumor ICD, we analyzed the ER stress-related signature levels from cancer cells of FK228 pre- and post-treated tumors according to scRNA-seq data. GO enrichment analyses showed that the ER stress pathway was obviously upregulated in cancer cells from FK228-treated tumors (Fig. 6A). The phosphorylation of eIF2α protein is

Fig. 5 FK228 enhances response to anti-PD-L1 immunotherapy and reshapes tumor immune microenvironment leading to tumor inhibition. A Diagram of the combination therapy with FK228 and anti-PD-L1 inhibitor. CT26 tumor-bearing mice (4×10^5 cells) were constructed. These tumor-bearing mice were injected with indicated agents *via* the tail vein, when the tumor volume attained to approximately 50 mm^3. After the indicated treatments, the tumors were harvested and used to further analyses. **B** Representative images of the tumors isolated from the CT26 subcutaneous tumor model mice receiving the indicated administration ($n = 5$). Scale bar, 1 cm. **C** Spider plots of tumor volume in each group with indicated administration. Each line served as one mouse ($n = 10$). **D** Weights of the tumors tissues from mice receiving the indicated administration ($n = 5$). Significant difference was executed using Student's *t*-test. **E** Survival rates of mice with indicated administration ($n = 6$ for DMSO+IgG, DMSO + @PD-L1, FK228+IgG, and $n = 11$ for FK228 + @PD-L1). Significant difference was executed using Log-rank (Mantel-Cox) test. **F** Ro/e heatmap showing the combined treatment preference of each cell subtype. Significant difference was executed using chi-square test. **G** The percentages of pro-inflammatory Mφ, DC, NK and CD8$^+$ T cells in tumor tissues from mice with indicated administration. Significant difference was executed using Student's *t*-test. **H, I** Representative immunofluorescence image of CD8$^+$ T cells (**H**), and pro-inflammatory or anti-inflammatory Mφs (**I**) in tumor tissues treated with indicated administration. Scale bar, 50 μm. **J** Standardized mean expressions of cytotoxic granules in CD8$^+$ T cells grouped by combined treatment. **K** The amount of activated CD8$^+$ T cells with high expression of GZMB in tumor tissues from pre- and post-combined treated mice. Significant difference was executed using Student's *t*-test.

one of the classic hallmarks of ER stress [41]. Next, we evaluated the phosphorylated eIF2α levels in FK228-treated MC38, CT26, and 4T1 cells using western blotting, and the results showed that the phosphorylation levels of eIF2α at serine 49 and 51 robustly increased with FK228 incubation time and reached peak value at 24 h (Figs. 6B and S12). Subsequently, a rescue assay using 4-Phenylbutyric acid (4-PBA), an ER stress inhibitor [50], in the abovementioned three solid tumor cell lines treated with FK228 was conducted. We observed the greatly recovered cell viability in FK228-treated tumor cells during 4-PBA supplementation (Fig. 6C). The obviously reducing death cells existed in 4-PBA rescued FK228-treated tumor cells groups in accordance with 7-AAD staining analyses (Fig. 6D). To further explore the relationship between ER stress and necroptosis, we investigated the expressions of two hallmark (phosphorylated- eIF2α and RIP3) about ER stress and necroptosis in solid tumor cells with or without FK228 and/or 4-PBA administration. Both eIF2α and RIP3 simultaneously exhibited dramatic phosphorylation in the single FK228 treatment group, while 4-PBA supplementation significantly decreased their phosphorylation levels (Figs. 6E and S13). These investigations demonstrated that FK228-induced necroptosis was attributed to ER stress.

DISCUSSION
Accumulating clinical trials have illustrated that FK228 is a highly promising HDACi for treating non-solid tumors [51, 52]. According to global cancer statistics in 2022, the new cases and deaths for non-solid tumors accounted for only 6.5% and 7.1%, respectively [53]. Numerous solid tumor cases might not benefit from FK228 therapy. As early as the 1990s, Ueda et al. reported the tremendous solid tumor cell inhibition by FK228 using in vitro cell experiments and in vivo immunodeficient xenograft nude mouse models [6, 35]. Subsequently, there is a growing interest in solid tumor therapy using FK228. After 30 years of development, approximate 18 clinical trials of FK228 for the treatment of solid tumors have been conducted (Table S2) *via* a systematic search of clinical trial website (www.clinicaltrials.gov). However, six published clinical trials demonstrated the moderate therapeutic efficacy of a single FK228 treatment in solid tumors. We further found that these clinical studies have several shortcomings in terms of experimental design. For example, patients who had developed resistance to other drugs were selected for a clinical study of colorectal cancer, while FK228 is served as a substrate of both multidrug resistance-associated protein (MRP1) and P-glycoprotein [6]. Although FK228 monotherapy exhibited a modest level of antitumor activity in a phase II for metastatic castration-resistant prostate cancer, two patients who have received standard hormone treatments showed significant anti-tumor responses after FK228 treatments, indicating that FK228 when combined with other agents could have extremely clinical activity in solid tumor therapy [7].

Previous studies have shown that FK228 directly inhibits tumor growth by the cell cycle arrests and apoptosis inductions in tumor cells [4, 54]. Interestingly, our research found that FK228 can induce ER stress in tumor cells, thereby triggering their necroptosis. In programmed cell death, the signaling pathways for apoptosis and necroptosis share some overlapping molecular components, such as the upstream Fas/TNFR receptor family, while the main differences are the involved intracellular signaling molecules [38]. In this study, we used the corresponding inhibitors for the intracellular signaling molecules associated with these two cell death types [37, 55]. These results clearly indicated that the addition of necroptosis-specific inhibitor significantly reversed the decline in cell viability mediated by FK228, whereas the same phenomenon was not observed in the apoptosis-specific inhibitor group. Previous investigation has shown FK228-mediated ER stress by class I HDAC-dependent mechanism [56]. Programming cell death, such as necroptosis and ferroptosis, is also associated with ICD and immune responses [57, 58]. ER stress-mediated necroptosis often results in the release of a large amount of DAMPs and pro-inflammatory contents in tumor cells, thereby eliciting the occurrence of ICD in entire tumor tissues [41, 59]. Impressively, we also confirmed the FK228-induced ICD through in vivo and in vitro experiments. Therefore, FK228-induced ER stress is likely due to the class I HDAC-dependent pathway, which further leads to necroptosis and ICD activity.

Beyond the direct tumor cell inhibition, FK228 can regulate the TIME of solid tumors *via* ICD induction [15, 17]. Unfortunately, few studies have comprehensively reported on the panoramic view of the TIME of FK228-treated solid tumors. In our case, we performed scRNA-seq to characterize the TIME landscape of FK228 pre- and post- treatment solid tumors. Our results revealed that many immune cell subgroups undergo significant changes after FK228 administration, including increased infiltration and activity of antitumor immune cells, and decreased protumor immune cells. Many studies have shown that enough tumor-infiltrating T cells are favorable for patient survival [17, 60]. During analyzing T cell subtypes, we observed the abundant anticancer CD8$^+$ T cell infiltration in FK228-treated solid tumors. The chemokine CXCL10 can attract T cells into solid tumors, which promotes a better response to anticancer therapy [61]. Additionally, CX3CL1 serves as a chemoattractant for T cells, monocytes, and NK cells, while also promoting adhesion between these immune cells and tumor cells [62]. Based on Luminex platform, our investigation revealed that after treatment with FK228, the levels of CXCL10 and/or CX3CL1 released by tumor cells significantly increased. Moreover, the activation of CD8$^+$ T cells is crucial for anticancer effects. Activated cytotoxic CD8$^+$ T cells can secrete perforin, granzymes and IFN-γ, which damage the target-tumor cell membrane and kill cancer cells [47, 63]. We analyzed the expression of cytotoxic granules in CD8$^+$ T cells infiltrating into mouse solid tumors after FK228 treatment and found a significant increase in the expression of cytotoxic molecules, including the granzyme family,
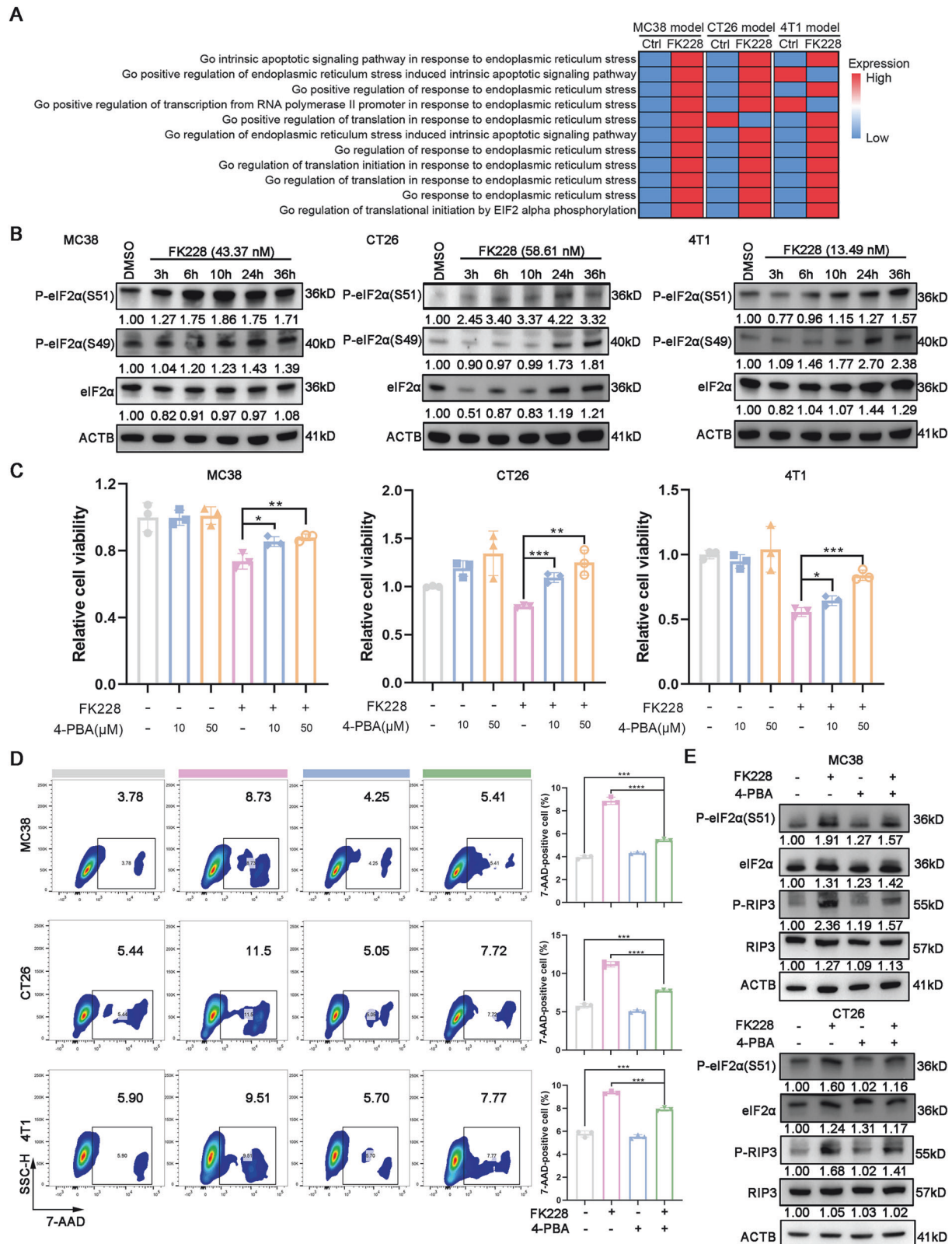
Fig. 6 FK228 activates endoplasmic reticulum (ER) stress of solid tumor cells resulting in necroptosis. A Standardized mean levels of endoplasmic reticulum stress related signatures in tumor cells grouped by FK228 pre- and post-treatment. Ctrl indicates DMSO treatment. **B** Western blotting showing the classic hallmarks expression of ER stress. **C** The cell viability of solid tumors treated with FK228 and subsequently recovered with 4-Phenylbutyric acid (4-PBA) using the CCK-8 assay. Solid tumor cells were exposed to FK228 at its IC$_{50}$ concentrations and/or 4-PBA at doses of 10 μM or 50 μM for a duration of 24 h. Following treatment, cell survival was evaluated using the CCK-8 assay. Significant difference was executed using Student's t-test. **D** Solid tumor cell death by FK228-induction after 4-PBA rescue using 7-AAD staining. Significant difference was executed using Student's t-test. **E** Western blotting showing ER stress-mediated necroptosis.

perforin, and IFN-γ. As FK228 is an epigenetic drug, it may activate transcription factors that regulate the expressions of the above cytotoxic granules. Subsequently, using transcription regulation analysis, we identified a series of upregulated transcription factors, such as *Runx3* and *Nfkb2*, in CD8^{+} T cells from FK228-treated mouse solid tumors. In line with these findings, previous ATAC-seq analyses of CD8^{+} T cells showed Runx3 can access the *Gzmb* gene, thereby delaying tumor growth [64]. These results suggest that FK228 not only induces infiltration of CD8^{+} T cells but also directly regulates transcription factors within these cells, resulting in the release of cytotoxic granules.

Besides regulating T cells, FK228 can affect myeloid cells, especially macrophages. Our original discovery revealed that FK228 can directly reprogram TAMs into pro-inflammatory Mφs (M1-like). Furthermore, the HDACi entinostat remodeled tumor-infiltrating MDSCs to enhance both T cell activation and infiltration [12]. MDSCs are involves in the formation of an immunosuppressive TIME that severely hinders the infiltration and sensitization of effector immune cells, causing tolerogenic immunological effects [61]. We found that FK228 can reduce MDSC infiltration, which might unleash T cell activation. Impressively, we and other groups have demonstrated that FK228 can promote the expression of the immune checkpoint PD-L1 on tumor cells [15, 16]. In addition, we found that FK228 can also increase the expression of PD-1 on CD8^{+} T cells, and the PD-1/PD-L1 axis has the potential to lead to CD8^{+} T cell exhaustions [47]. Recent studies have also revealed the presence of a subset of CD8^{+} T cells with both activated and exhausted-like phenotypes in solid tumors, and the TIME enriched with these cell types shows increased sensitivity to ICB [17, 43, 44]. Following FK228 treatment, solid tumors, including immune-cold tumors, increased the activated and exhausted-like CD8^{+} T cells, suggesting the ability of FK228 to improve the effectiveness of ICB. Therefore, we explored the combination of FK228 with PD-L1 inhibition in an immune-cold tumor CT26-bearing mouse model. After combined treatment, the tumors in the mice were almost completely inhibited, with some tumors showing regression. We comprehensively presented the single-cell landscape of FK228-treated solid tumors and investigated the pathways by which FK228 alters the TIME. The deeper mechanisms of FK228-mediated TIME reprogramming need to be further investigated in future studies, such as how FK228 polarizes TAMs into pro-inflammatory Mφs, and regulates the transcription factors that promote the expression of cytotoxic granules in CD8^{+} T cells. Strikingly, we noted that Tregs increased in the combination treatment group. Indeed, the increased intratumoral infiltration of global T cells was observed following either PD-L1 inhibitor or FK228 administration. Notably, a further increase in global T cell infiltration were detected in tumors from mice with combination therapy. The proportion alteration patterns of Treg cells were similar to those of total T cell numbers, indicating that increased Treg cell infiltration was a consequence of alterations in the total T cell number. Insightly, in cellular immunity, T and NK cells use perforin to deliver serine protease granzymes into cancer cells to kill them, executing pyroptosis, a form of pro-inflammatory cell death [65]. Hence, this pyroptosis probably combined with FK228-induced immunogenic cell death to further enhance global T cell infiltration.

In conclusion, our study firstly provides a novel mechanism and the single-cell landscapes of FK228-induced TIME remodeling in solid tumors. This histone deacetylase inhibitor turns the unfavorable TIME into a favorable TIME, contributing to enhancing the efficacy of immunotherapy in solid tumors. In line with this notion, our findings highlight FK228 as a novel ICB sensitizer that could be considered to synergize with ICB in solid tumors in the future. Currently, many clinical trials have not been completed. Our investigation of FK228 in solid tumor therapy provides a reference for improving current clinical studies.

DATA AVAILABILITY

REFERENCES
1. FDA. StatBite: FDA oncology drug product approvals in 2009. J Natl Cancer Inst. 2010;102:219.
2. Vu K, Wu CH, Yang CY, Zhan A, Cavallone E, Berry W, et al. Romidepsin plus liposomal doxorubicin is safe and effective in patients with relapsed or refractory T-cell lymphoma: results of a phase I dose-escalation study. Clin Cancer Res. 2020;26:1000–8.
3. Blanchard F, Kinzie E, Wang Y, Duplomb L, Godard A, Held WA, et al. FR901228, an inhibitor of histone deacetylases, increases the cellular responsiveness to IL-6 type cytokines by enhancing the expression of receptor proteins. Oncogene. 2002;21:6264–77.
4. Furumai R, Matsuyama A, Kobashi N, Lee KH, Nishiyama M, Nakajima H, et al. FK228 (depsipeptide) as a natural prodrug that inhibits class I histone deacetylases. Cancer Res. 2002;62:4916–21.
5. Gong K, Wang M, Duan Q, Li G, Yong D, Ren C, et al. High-yield production of FK228 and new derivatives in a Burkholderia chassis. Metab Eng. 2023;75:131–42.
6. Whitehead RP, Rankin C, Hoff PM, Gold PJ, Billingsley KG, Chapman RA, et al. Phase II trial of romidepsin (NSC-630176) in previously treated colorectal cancer patients with advanced disease: a Southwest Oncology Group study (S0336). Invest N. Drugs. 2009;27:469–75.
7. Molife LR, Attard G, Fong PC, Karavasilis V, Reid AH, Patterson S, et al. Phase II, two-stage, single-arm trial of the histone deacetylase inhibitor (HDACi) romidepsin in metastatic castration-resistant prostate cancer (CRPC). Ann Oncol. 2010;21:109–13.
8. Stadler WM, Margolin K, Ferber S, McCulloch W, Thompson JA. A phase II study of depsipeptide in refractory metastatic renal cell cancer. Clin Genitourin Cancer. 2006;5:57–60.
9. Arpinati L, Carradori G, Scherz-Shouval R. CAF-induced physical constraints controlling T cell state and localization in solid tumours. Nat Rev Cancer. 2024;24:676–93.
10. Xu T, Fang Y, Gu Y, Xu D, Hu T, Yu T, et al. HDAC inhibitor SAHA enhances antitumor immunity via the HDAC1/JAK1/FGL1 axis in lung adenocarcinoma. J Immunother Cancer. 2024;12:e010077.
11. Lisiero DN, Soto H, Everson RG, Liau LM, Prins RM. The histone deacetylase inhibitor, LBH589, promotes the systemic cytokine and effector responses of adoptively transferred CD8+ T cells. J Immunother Cancer. 2014;2:8.
12. Christmas BJ, Rafie CI, Hopkins AC, Scott BA, Ma HS, Cruz KA, et al. Entinostat converts immune-resistant breast and pancreatic cancers into checkpoint-responsive tumors by reprogramming tumor-infiltrating MDSCs. Cancer Immunol Res. 2018;6:1561–77.
13. Sun T, Liu B, Cai L, Zhou Y, Yang W, Li Y. Suberanilohydroxamic acid (SAHA), a HDAC inhibitor, suppresses the effect of Treg cells by targeting the c-Myc/CCL1 pathway in glioma stem cells and improves PD-L1 blockade therapy. J Neurooncol. 2024;168:457–71.
14. Gao Y, Nihira NT, Bu X, Chu C, Zhang J, Kolodziejczyk A, et al. Acetylation-dependent regulation of PD-L1 nuclear translocation dictates the efficacy of anti-PD-1 immunotherapy. Nat Cell Biol. 2020;22:1064–75.
15. Shi Y, Fu Y, Zhang X, Zhao G, Yao Y, Guo Y, et al. Romidepsin (FK228) regulates the expression of the immune checkpoint ligand PD-L1 and suppresses cellular immune functions in colon cancer. Cancer Immunol Immunother. 2021;70:61–73.
16. Kuo MH, Chen PY, Yang YP, Zheng MY, Miao CC, Wen KC, et al. Cytokine and epigenetic regulation of programmed death-ligand 1 in stem cell differentiation and cancer cell plasticity. Stem Cells. 2021;39:1298–309.
17. Zheng H, Zhao W, Yan C, Watson CC, Massengill M, Xie M, et al. HDAC Inhibitors Enhance T-Cell Chemokine Expression and Augment Response to PD-1 Immunotherapy in Lung Adenocarcinoma. Clin Cancer Res. 2016;22:4119–32.
18. Yang Y, Chen X, Pan J, Ning H, Zhang Y, Bo Y, et al. Pan-cancer single-cell dissection reveals phenotypically distinct B cell subtypes. Cell. 2024;187:4790–811.e22.
19. Liu B, Li S, Cheng Y, Song P, Xu M, Li Z, et al. Distinctive multicellular immunosuppressive hubs confer different intervention strategies for left- and right-sided colon cancers. Cell Rep. Med. 2024;5:101589.
20. Cui K, Yao S, Liu B, Sun S, Gong L, Li Q, et al. A novel high-risk subpopulation identified by CTSL and ZBTB7B in gastric cancer. Br J Cancer. 2022;127:1450–60.
21. Cui K, Gong L, Zhang H, Chen Y, Liu B, Gong Z, et al. EXOSC8 promotes colorectal cancer tumorigenesis via regulating ribosome biogenesis-related processes. Oncogene. 2022;41:5397–410.

22. Tian L, Gong L, Hao C, Feng Y, Yao S, Fei B, et al. ELOA promotes tumor growth and metastasis by activating RBP1 in gastric cancer. Cancer Med. 2023;12:18946–59.

23. Hossain DMS, Javaid S, Cai M, Zhang C, Sawant A, Hinton M, et al. Dinaciclib induces immunogenic cell death and enhances anti-PD1-mediated tumor suppression. J Clin Invest. 2018;128:644–54.

24. Wang Z, Chen J, Hu J, Zhang H, Xu F, He W, et al. cGAS/STING axis mediates a topoisomerase II inhibitor-induced tumor immunogenicity. J Clin Invest. 2019;129:4850–62.

25. Sun L, Liu R, Wu ZJ, Liu ZY, Wan AH, Yan S, et al. Galectin-7 induction by EHMT2 inhibition enhances immunity in microsatellite stability colorectal cancer. Gastroenterology. 2024;166:466–82.

26. Chen Y, Gong L, Cao Y, Liu Z, Wang Y, Cheng H, et al. Reprogramming tumor-associated macrophages by a dually targeted milk exosome system as a potent monotherapy for cancer. J Controlled Release. 2024;366:395–409.

27. Li A, Gong Z, Long Y, Li Y, Liu C, Lu X, et al. Lactylation of LSD1 is an acquired epigenetic vulnerability of BRAFi/MEKi-resistant melanoma. Dev Cell. 2025;60:1974–90.

28. Gong L, Tian L, Cui K, Chen Y, Liu B, Li D, et al. An off-the-shelf small extracellular vesicle nanomedicine for tumor targeting therapy. J Control Release. 2023;364:672–86.

29. Gong L, Li Y, Cui K, Chen Y, Hong H, Li J, et al. Nanobody-Engineered Natural Killer Cell Conjugates for Solid Tumor Adoptive Immunotherapy. Small. 2021;17:e2103463.

30. Hao Y, Hao S, Andersen-Nissen E, Mauck WM 3rd, Zheng S, Butler A, et al. Integrated analysis of multimodal single-cell data. Cell. 2021;184:3573–3587 e3529.

31. Cheng S, Li Z, Gao R, Xing B, Gao Y, Yang Y, et al. A pan-cancer single-cell transcriptional atlas of tumor infiltrating myeloid cells. Cell. 2021;184:792–809 e723.

32. Van de Sande B, Flerin C, Davie K, De Waegeneer M, Hulselmans G, Aibar S, et al. A scalable SCENIC workflow for single-cell gene regulatory network analysis. Nat Protoc. 2020;15:2247–76.

33. Andreatta M, Carmona SJ. UCell: Robust and scalable single-cell gene signature scoring. Comput Struct Biotechnol J. 2021;19:3796–8.

34. Safari M, Litman T, Robey RW, Aguilera A, Chakraborty AR, Reinhold WC, et al. R-Loop-Mediated ssDNA Breaks Accumulate Following Short-Term Exposure to the HDAC Inhibitor Romidepsin. Mol Cancer Res. 2021;19:1361–74.

35. Ueda H, Manda T, Matsumoto S, Mukumoto S, Nishigaki F, Kawamura I, et al. FR901228, a novel antitumor bicyclic depsipeptide produced by Chromobacterium violaceum No. 968. III. Antitumor activities on experimental tumors in mice. J Antibiot. 1994;47:315–23.

36. Sun JY, Wang JD, Wang X, Liu HC, Zhang MM, Liu YC, et al. Marine-derived chromopeptide A, a novel class I HDAC inhibitor, suppresses human prostate cancer cell proliferation and migration. Acta Pharm Sin. 2017;38:551–60.

37. Lin JF, Hu PS, Wang YY, Tan YT, Yu K, Liao K, et al. Phosphorylated NFS1 weakens oxaliplatin-based chemosensitivity of colorectal cancer by preventing PANoptosis. Signal Transduct Target Ther. 2022;7:54.

38. Newton K, Strasser A, Kayagaki N, Dixit VM. Cell death. Cell. 2024;187:235–56.

39. Tao P, Sun J, Wu Z, Wang S, Wang J, Li W, et al. A dominant autoinflammatory disease caused by non-cleavable variants of RIPK1. Nature. 2020;577:109–14.

40. Krysko DV, Garg AD, Kaczmarek A, Krysko O, Agostinis P, Vandenabeele P. Immunogenic cell death and DAMPs in cancer therapy. Nat Rev Cancer. 2012;12:860–75.

41. Wang L, Guan R, Xie L, Liao X, Xiong K, Rees TW, et al. An ER-targeting iridium(III) complex that induces immunogenic cell death in non-small-cell lung cancer. Angew Chem Int Ed Engl. 2021;60:4657–65.

42. Kumari N, Choi SH. Tumor-associated macrophages in cancer: recent advancements in cancer nanoimmunotherapies. J Exp Clin Cancer Res. 2022;41:68.

43. Mietz J, Kaulfuss M, Egli L, Opitz L, Munz C, Chijioke O. Human effector CD8(+) T cells with an activated and exhausted-like phenotype control tumour growth in vivo in a humanized tumour model. EBioMedicine. 2024;106:105240.

44. Cillo AR, Cardello C, Shan F, Karapetyan L, Kunning S, Sander C, et al. Blockade of LAG-3 and PD-1 leads to co-expression of cytotoxic and exhaustion gene modules in CD8(+) T cells to promote antitumor immunity. Cell. 2024;187:4373–4388 e4315.

45. Cassetta L, Pollard JW. Targeting macrophages: therapeutic approaches in cancer. Nat Rev Drug Discov. 2018;17:887–904.

46. Ma RY, Black A, Qian BZ. Macrophage diversity in cancer revisited in the era of single-cell omics. Trends Immunol. 2022;43:546–563.

47. Andrews LP, Butler SC, Cui J, Cillo AR, Cardello C, Liu C, et al. LAG-3 and PD-1 synergize on CD8(+) T cells to drive T cell exhaustion and hinder autocrine IFN-gamma-dependent anti-tumor immunity. Cell. 2024;187:4355–4372 e4322.

48. Sen Santara S, Lee DJ, Crespo A, Hu JJ, Walker C, Ma X, et al. The NK cell receptor NKp46 recognizes ecto-calreticulin on ER-stressed cells. Nature. 2023;616:348–56.

49. King AP, Wilson JJ. Endoplasmic reticulum stress: an arising target for metal-based anticancer agents. Chem Soc Rev. 2020;49:8113–36.

50. Wu S, Wang B, Li H, Wang H, Du S, Huang X, et al. Targeting STING elicits GSDMD-dependent pyroptosis and boosts anti-tumor immunity in renal cell carcinoma. Oncogene. 2024;43:1534–48.

51. Zinzani PL, Pellegrini C, Cerciello G, Monaco F, Volpetti S, Peli A, et al. Romidepsin in relapsed/refractory T-cell lymphomas: Italian experience and results of a named patient program. Leuk Lymphoma. 2016;57:2370–4.

52. Luan Y, Li X, Luan Y, Luo J, Dong Q, Ye S, et al. Therapeutic challenges in peripheral T-cell lymphoma. Mol Cancer. 2024;23:2.

53. Bray F, Laversanne M, Sung H, Ferlay J, Siegel RL, Soerjomataram I, et al. Global cancer statistics 2022: GLOBOCAN estimates of incidence and mortality worldwide for 36 cancers in 185 countries. CA Cancer J Clin. 2024;74:229–63.

54. Saijo K, Katoh T, Shimodaira H, Oda A, Takahashi O, Ishioka C. Romidepsin (FK228) and its analogs directly inhibit phosphatidylinositol 3-kinase activity and potently induce apoptosis as histone deacetylase/phosphatidylinositol 3-kinase dual inhibitors. Cancer Sci. 2012;103:1994–2001.

55. Degterev A, Huang Z, Boyce M, Li Y, Jagtap P, Mizushima N, et al. Chemical inhibitor of nonapoptotic cell death with therapeutic potential for ischemic brain injury. Nat Chem Biol. 2005;1:112–9.

56. Hui KF, Chiang AK. Combination of proteasome and class I HDAC inhibitors induces apoptosis of NPC cells through an HDAC6-independent ER stress-induced mechanism. Int J Cancer. 2014;135:2950–61.

57. Meier P, Legrand AJ, Adam D, Silke J. Immunogenic cell death in cancer: targeting necroptosis to induce antitumour immunity. Nat Rev Cancer. 2024;24:299–315.

58. Cui K, Wang K, Huang Z. Ferroptosis and the tumor microenvironment. J Exp Clin Cancer Res. 2024;43:315.

59. Taft J, Markson M, Legarda D, Patel R, Chan M, Malle L, et al. Human TBK1 deficiency leads to autoinflammation driven by TNF-induced cell death. Cell. 2021;184:4447–4463 e4420.

60. Zhang L, Conejo-Garcia JR, Katsaros D, Gimotty PA, Massobrio M, Regnani G, et al. Intratumoral T cells, recurrence, and survival in epithelial ovarian cancer. N Engl J Med. 2003;348:203–13.

61. Conche C, Finkelmeier F, Pesic M, Nicolas AM, Bottger TW, Kennel KB, et al. Combining ferroptosis induction with MDSC blockade renders primary tumours and metastases in liver sensitive to immune checkpoint blockade. Gut. 2023;72:1774–82.

62. Navarro-Gonzalez JF, Mora-Fernandez C, Muros de Fuentes M, Garcia-Perez J. Inflammatory molecules and pathways in the pathogenesis of diabetic nephropathy. Nat Rev Nephrol. 2011;7:327–40.

63. Wang W, Green M, Choi JE, Gijon M, Kennedy PD, Johnson JK, et al. CD8(+) T cells regulate tumour ferroptosis during cancer immunotherapy. Nature. 2019;569:270–4.

64. Milner JJ, Toma C, Yu B, Zhang K, Omilusik K, Phan AT, et al. Runx3 programs CD8(+) T cell residency in non-lymphoid tissues and tumours. Nature. 2017;552:253–7.

65. Zhou Z, He H, Wang K, Shi X, Wang Y, Su Y et al. Granzyme A from cytotoxic lymphocytes cleaves GSDMB to trigger pyroptosis in target cells. Science. 2020;368.

AUTHOR CONTRIBUTIONS
LG, and YMZ conceptualized the study. LG, LT, HL, KXZ, and SX performed the experiments and analyzed the data. KSC performed the in-silico analysis and visualization for all scRNA-seq. LG, KSC and ZCG proposed the hypothesis of mechanism. YMZ supervised the study. LG wrote the draft manuscript. LG, HCH, YZZ, KSC and ZCG revised the manuscript. All authors approved to the final version and submit this manuscript.

COMPETING INTERESTS
The authors declare no competing interests.

ETHICS APPROVAL AND CONSENT TO PARTICIPATE

All animal protocols were reviewed and approved by the Institutional Animal Care and Use Committee of Shenzhen Institutes of Advanced Technology, Chinese Academy of Science (SIAT-IACUC-240122-HCS-GL-A2459). Humans-related experiment does not apply to this study.

ADDITIONAL INFORMATION

Supplementary information The online version contains supplementary material available at https://doi.org/10.1038/s41388-025-03558-y.

Correspondence and requests for materials should be addressed to Zhicheng Gong, Kaisa Cui or Youming Zhang.

Reprints and permission information is available at http://www.nature.com/reprints

Publisher's note Springer Nature remains neutral with regard to jurisdictional claims in published maps and institutional affiliations.